

Electronic Structure of Pyrochlore Iridates: From Topological Dirac Metal to Mott Insulator

Xiangang Wan¹, Ari Turner², Ashvin Vishwanath^{2,3}, Sergey Y. Savrasov^{1,4}

¹*National Laboratory of Solid State Microstructures and Department of Physics, Nanjing University, Nanjing 210093, China*

²*Department of Physics, University of California, Berkeley, CA 94720*

³*Materials Sciences Division, Lawrence Berkeley National Laboratory, Berkeley CA 94720.*

⁴*Department of Physics, University of California, Davis, One Shields Avenue, Davis, CA 95616.*

In $5d$ transition metal oxides such as the iridates, novel properties arise from the interplay of electron correlations and spin-orbit interactions. We investigate the electronic structure of the pyrochlore iridates, (such as $\text{Y}_2\text{Ir}_2\text{O}_7$) using density functional theory, LDA+U method, and effective low energy models. A remarkably rich phase diagram emerges on tuning the correlation strength U . The Ir magnetic moment are always found to be non-collinearly ordered. However, the ground state changes from a magnetic metal at weak U , to a Mott insulator at large U . Most interestingly, the intermediate U regime is found to be a Dirac semi-metal, with vanishing density of states at the Fermi energy. It also exhibits topological properties - manifested by special surface states in the form of Fermi arcs, that connect the bulk Dirac points. This Dirac phase, a three dimensional analog of graphene, is proposed as the ground state of $\text{Y}_2\text{Ir}_2\text{O}_7$ and related compounds. A narrow window of magnetic ‘axion’ insulator, with axion parameter $\theta = \pi$, may also be present at intermediate U . An applied magnetic field induces ferromagnetic order and a metallic ground state.

Previously, some of the most striking phenomena in solids, such as high temperature superconductivity[1] and colossal magnetoresistance[2] were found in transition metal systems involving $3d$ orbitals, with strong electron correlations. Now it has been realized that in $4d$ and the $5d$ systems, whose orbitals are spatially more extended, a regime of intermediate correlation appears. Moreover, they display significant spin-orbit coupling, which modifies their electronic structure as recently verified in Sr_2IrO_4 [3]. This is a largely unexplored domain, but already tantalizing new phenomena have been glimpsed. For example, in the $5d$ magnetic insulator, Na_2IrO_3 [4], a disordered ground state persists down to the lowest measured temperatures, making it a prime candidate for a quantum spin liquid[5].

It is known that strong spin-orbit interactions can lead to a novel phase of matter, the topological insulator[6]. However, the experimental candidates uncovered so far have weak electron correlations. Recently, it was realized that the iridates are promising candidates to realize topological insulators[7], and that Iridium based pyrochlores in particular [8], provide a unique opportunity to study the interplay of Coulomb interactions, spin-orbit coupling and the band topology of solids.

The pyrochlore iridates, with general formula $A_2\text{Ir}_2\text{O}_7$, where $A = \text{Yttrium}$, or a Lanthanide element, will be the main focus of this work. Both the A and Ir atoms are located on a network of corner sharing tetrahedra [9, 10]. Pioneering experiments[11] on the pyrochlore iridates, revealed an evolution of ground state properties with increasing radius of the A ion, which is believed to tune electron correlations. While $A = \text{Pr}$ is metallic, $A = \text{Y}$ is an insulator as low temperatures. Subsequently, it was shown that the insulating ground states evolve from a high temperature metallic phase, via a magnetic

transition[12, 13]. The magnetism was shown to arise from the Ir sites, since it also occurs in $A = \text{Y, Lu}$, where the A sites are non-magnetic. While its precise nature remains unknown, the absence of a net moment rules out ferromagnetism.

We show that electronic structure calculations can naturally account for this evolution and points to a novel ground state whose properties are described here. First, we find that magnetic moments order on the Ir sites in a non-collinear pattern with moment on a tetrahedron pointing all-in or all-out from the center. This structure retains inversion symmetry, a fact that greatly aids the electronic structure analysis. While the magnetic pattern remains fixed, the electronic properties evolve with correlation strength. For weak correlations, or in the absence of magnetic order, a metal is obtained, in contrast to the interesting topological insulator scenario of Ref. [8]. With strong correlations we find a Mott insulator, with all-in/all-out magnetic order. However, for the case of intermediate correlations, relevant to $\text{Y}_2\text{Ir}_2\text{O}_7$, the electronic ground state is found to be an unusual *Dirac semi-metal*, with linearly dispersing Dirac nodes at the chemical potential. Indeed, this dispersion is analogous to graphene[14], but occurs inside a three dimensional magnetic solid. The small density of states leads to a vanishing conductivity at low temperatures. The Dirac fermions here are rather different from those in three dimensional semi-metals such as elemental Bismuth, which are inversion symmetric and non-magnetic. Here, the Dirac fermions at a particular momentum are described by a handedness (which is left or right handed), and a two component wavefunction. They cannot be gapped unless they mix with a fermion of opposite handedness. In contrast, Dirac fermions in Bismuth have four component wavefunctions, no particular handedness, and are

typically gapped. Such a three dimensional electronic structure has, to our knowledge, not been discussed before.

A key property of this Dirac semi-metal phase of two component Dirac fermions, is unusual band topology, reminiscent of topological insulators. Since the bulk fermi surface only consists of a set of momentum points, surface states can be defined for nearly every surface momentum, and are always found to occur on certain surfaces. They take the shape of ‘Fermi arcs’ in the surface Brillouin zone, that stretch between Dirac points. Hence we term this phase *topological Dirac metal*.

We also mention the possibility of an exotic insulating phase emerging when the Dirac points annihilate in pairs, as the correlation are reduced. This phase shows a topological magnetoelectric effect[15], captured by the magneto-electric parameter $\theta = \pi$, whose value is protected by the inversion symmetry. Since it is analogous to the axion vacuum in particle physics[16], so we call it the $\theta = \pi$ Axion insulator. Although our LSDA+U+SO calculations find that a metallic phase intervenes before this possibility is realized, we note that LDA systematically underestimates gaps, so this scenario could well occur in reality. Finally, we mention that modest magnetic fields could induce a reorientation of the magnetic moments, leading to a metallic phase. Our results are summarized in the phase diagram Figure 1. Previous studies considered ferromagnetism [17], and structural distortion [18] in iridates.

Our calculations suggest that new functionalities such as controlling electrical properties via magnetic textures, and field induced metallic states can be realized in these materials, with implications for spintronics, magneto-electrical and magneto-optical devices.

METHOD

We perform our electronic structure calculations based on local spin density approximation (LSDA) to density functional theory (DFT) with the full-potential, all-electron, linear-muffin-tin-orbital (LMTO) method[19]. We use LSDA+U scheme[20] to take into account the electron-electron interaction between Ir 5d electrons and vary parameter U between 0 and 3 eV for Ir 5d electrons to see what effects the on site Coulomb repulsion would bring to the electronic structure of Iridates. In general, we expect that U can be somewhere between 1 and 2 eV for the extended 5d states. When the A site is a rare earth element, we also add the Coulomb interaction for the localized 4f electrons and use U = 6 eV. We use a $24 \times 24 \times 24$ k-mesh to perform Brillouin zone integration, and switch off symmetry operations in order to minimize possible numerical errors in studies of various (non-)collinear configurations. We use experimental lattice parameters[12] in all set ups.

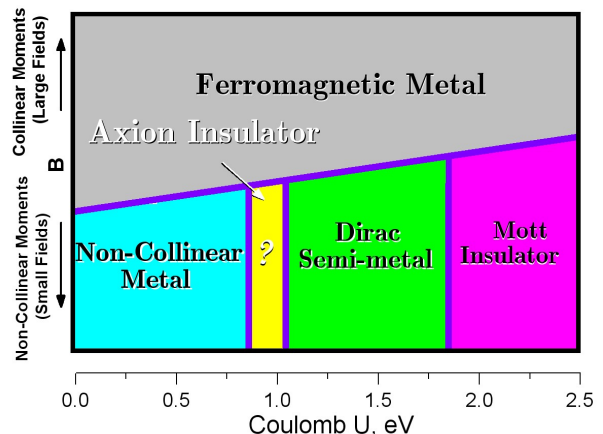


FIG. 1: Sketch of the phase diagram for pyrochlore iridates from our microscopic electronic structure calculation: Horizontal axis corresponds to the increasing interaction among Ir 5d electrons (the scale is obtained using LSDA+SO+U method) while the vertical axis corresponds to external magnetic field which aligns the moments and triggers a transition out of the zero field non-collinear “all-in/all-out” ground state. We find normal magnetic metal, Mott insulator and Dirac semi-metal phases, and also possibly an exotic insulator, a magnetic insulator with magneto-electric parameter $\theta = \pi$, which we label here as axion insulator.

Throughout, we exploit inversion symmetry which constrains the phase diagram, by tracking wavefunction parities at time reversal invariant momenta. Near electronic phase transitions, a low energy $k.p$ theory is developed to understand qualitative features of the neighboring phases. Finally, topological band theory based on momentum space Berry connections is utilized in deducing the physical properties of the phases.

MAGNETIC CONFIGURATION

We first study magnetic configuration and discuss our results for $\text{Y}_2\text{Ir}_2\text{O}_7$. Since the strength of the spin-orbit (SO) coupling is large for Ir 5d electrons, and leads to insulating behavior in Sr_2IrO_4 [3], we perform the LSDA+U+SO calculations. There are four Ir atoms inside the unit cell forming a tetrahedral network as shown in Fig.1 which is geometrically frustrated. Thus, we carry out several calculations with the initial state to be (i) ferromagnetic, with moment along (100), (111), (110) or (120) directions (ii) antiferromagnetic with two sites in a tetrahedron along and other two pointed oppositely to the directions above; non-collinear structures (iii) “all-in/out” pattern (where all moments point to or away from the centers of the tetrahedron see Fig 1), (iv) “2-in/2-out” (two moments in a tetrahedron point to the center of this tetrahedron, while the other two moments point away from the center, i.e. the spin-ice[21] configu-

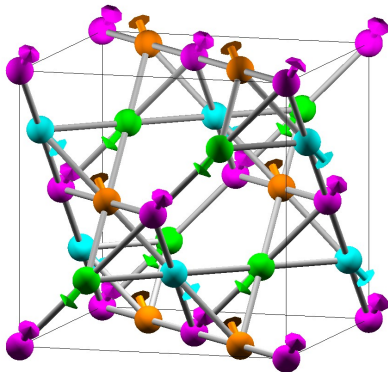


FIG. 2: The pyrochlore crystal structure showing Ir corner sharing tetrahedral network and the magnetic configuration corresponding to the "all-in/all-out" alignment of moments. A degenerate state is obtained on reversing the moments.

ration), and (v) "3-in/1-out" magnetic structures.

We find that the "all-in/out" configuration is the ground state. Different from other magnetic configurations, during the self-consistency the "all-in/out" state will retain their initial input direction; thus, there is no net magnetic moment. This is consistent with the absence of the magnetic hysteresis in experiments[12]. The all-in/all-out magnetic configuration was predicted to occur in pyrochlore antiferromagnets with Dzyaloshinsky-Moriya (D-M) interactions[22]. Symmetry dictates the form of D-M interactions except for the sign, which leads to two cases, direct and indirect D-M. The all-in/all-out state is the unique ground state for the former while the indirect D-M ground state is a coplanar state with the four spins being either antiparallel or orthogonal[22]. We find that the indirect D-M pattern has higher energy than the all-in/all-out state. This provides further evidence that the all-in/all-out spin configuration is the natural ground state.

The next lowest energy configuration is the ferromagnetic state. Interestingly, the rotation of magnetization does not cost much energy despite strong SO interactions. The (111) direction is found to be lowest ferromagnetic state, but the energy difference between this and the highest energy (001) state is just about 4.17 meV per unit cell. Also, all of them produce a considerable net magnetic moment in contrast to the experiment [11, 12, 23]. Our findings are summarized in Table I for a typical value of $U=1.5$ eV, and similar results are found for other values of U in the range from 0 to 3 eV. We find that the energy difference between the ground and several selected excited states with different orientations of moments is small. Therefore, modest magnetic fields may induce a transition into the ferromagnetic state.

TABLE I: The spin $\langle S \rangle$ and orbital $\langle O \rangle$ moment (in μ_B), the total energy E_{tot} (in meV) for several selected magnetic configurations of $Y_2Ir_2O_7$ as calculated using LSDA+U+SO method with $U=1.5$ eV. The IDM is a coplanar configuration predicted for one sign of D-M interactions in Ref. [22]

Configuration:	(001)	(111)	2-in/2-out	IDM	all-in/out
$\langle S \rangle$	0.08	0.10	0.09	0.06	0.13
$\langle O \rangle$	0.09	0.10	0.07	0.06	0.12
E_{tot} (meV)	5.47	1.30	3.02	2.90	0.00

ELECTRONIC PHASES AND WAVEFUNCTION PARITIES

We now discuss electronic properties of Iridates that emerge from our LSDA+U+SO calculations. A variety of phases ranging from normal metal at small U to Dirac semi-metallic at intermediate $U \sim 1.5$ eV and Mott insulating phase at U above 2 eV with non-collinear magnetic "all-in/out" ordering are predicted. Since pressure or chemical substitution may alter the screening and the electronic bandwidth resulting in changes in U we expect that these phases can be observed experimentally in iridates.

The basic features of the electronic structure can be understood by considering each of four Ir atoms in pyrochlore lattice which is octahedrally coordinated by six O atoms. This makes the Ir 5d state split into doubly degenerate e_g and triply degenerate t_{2g} states. Due to the extended nature of Ir 5d orbital, the crystal-field splitting between t_{2g} and e_g is large with the e_g band to be 2 eV higher than the Fermi level. The bands near the Fermi level are mainly contributed by Ir t_{2g} with some mixing with O 2p states. SO coupling has a considerable effect on these t_{2g} states: it lifts their degeneracy and produces quadruplet with $J_{eff} = 3/2$ and doublet with $J_{eff} = 1/2$ with the latter lying higher in energy. Alternatively, one can view the d-shell in strong SO limit which splits the 10 fold degenerate state onto lower lying $J = 3/2$ and higher lying $J = 5/2$ multiplets. A subsequent application of the cubic crystal field would leave the $J = 3/2$ multiplet degenerate but would split the 6-fold degenerate $J = 5/2$ state onto Γ_7 doublet and Γ_8 quadruplets. Since Ir occurs in its 4+ valence, its 5 electrons would fill completely $J = 3/2$ subshell and put an additional one electron into the Γ_7 doublet thought as the state with $J_{eff} = 1/2$ in some previous work [3]. For the solid, we thus expect 8 narrow energy bands at half-filling to appear in the vicinity of the chemical potential that correspond to the Γ_7 doublets of four Ir atoms.

The precise behavior of these electronic states depends on magnetic configuration. Our band structure calculations for collinear alignments of moments show metallic bands regardless the value of U that we use in our simulations. On the other hand, we find that the electronic states for the non-collinear "all-in/out" magnetic state

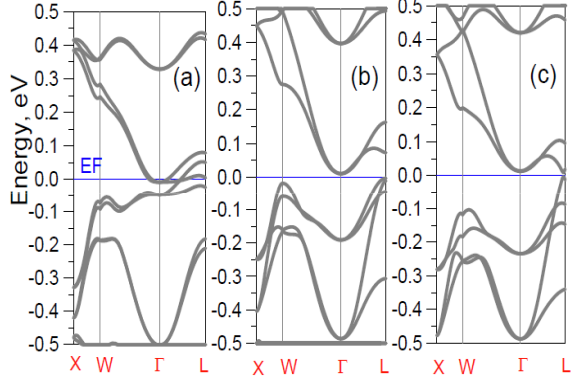


FIG. 3: Evolution of electronic band structure of $\text{Y}_2\text{Ir}_2\text{O}_7$ shown along high symmetry directions, calculated using LSDA+U+SO method with three different values of U equal (a) 0, (metallic) (b) 1.5 eV, and (c) 2 eV. (Insulator with small gap). The Dirac point that is present in case (b), is not visible along high symmetry lines.

depend strongly on the actual value of U used in the calculation. In particular, we predict that when U is less than 1 eV, the ground state is a normal metal while if U is about 1.8 eV or larger, we find the band structure to be insulating with an energy gap whose value depends on U .

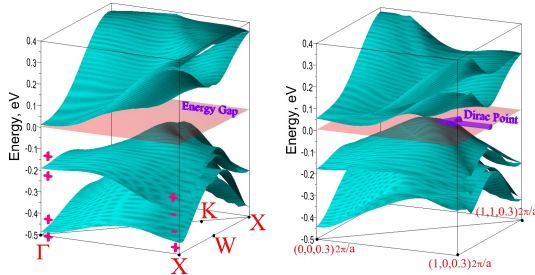


FIG. 4: Calculated energy bands in the vicinity of the Fermi level using LSDA+U+SO method with $U=1.5$ eV. on left: corresponds to plane $k_z = 0$ with band parities shown; (b) corresponds to plane $k_z = 0.32\pi/a$ where Dirac point is predicted to exist. The shaded plane is at the Fermi level.

Weak Correlations: An interesting recent study proposed a tight-binding model for the non-magnetic phase of the iridates, which was a topological insulator [8], a natural phase on the pyrochlore lattice [8, 24]. Our LDA studies of the realistic electronic structures contradict this, instead we find a metallic phase (see Fig. 3a). One can understand the discrepancy by analyzing the structure of energy levels at the Γ point (Brillouin Zone center) for the low energy 8-band complex, composed of the four $J_{\text{eff}} = 1/2$ states. In [8], these appear with degeneracies

TABLE II: Calculated parities of states at Time Reversal Invariant Momenta (TRIMs) for several electronic phases of the iridates. Only the top four filled levels are shown in order of increasing energy.

Phase	Γ	X, Y, Z	L'	$L (\times 3)$
$U=2.0$, all-in (Mott)	+	+	+	+
$U=1.5$, all-in (Dirac)	+	+	+	+
$U=2.0$, 111-Ferro	+	+	+	+

4,2,2 which after filling with 4 electrons results in an insulating band structure. Our study of the non-magnetic state using LDA+SO method (with no U) results, on the other hand, in the sequence 2,4,2 of degeneracies, which is necessarily metallic assuming 4 levels are filled. Thus, one needs either magnetic order, or a structural transition[18], to recover an insulating phase.

Strong Correlations and the Mott Limit: When $U > 1.8\text{eV}$, an insulating band structure is obtained with the all-in/all-out magnetic configuration, as shown in the figure 3c. Indeed, it remains qualitatively similar on increasing U to large values, where a site localized moment is expected, i.e. the Mott insulator. This can be further verified by calculating the parity eigenvalues. Note that all the magnetic structures considered above preserve *inversion* (or parity) symmetry. Thus, if we pick e.g. an Iridium atom as the origin of our coordinate system, then inversion $\mathbf{r} \rightarrow -\mathbf{r}$ leaves the crystal structure and magnetic pattern invariant. This implies a relation between crystal momenta $\pm\mathbf{k}$. At special momenta, called TRIMs (Time Reversal Invariant Momenta), that are invariant under inversion, we can label states by parity eigenvalues $\xi = \pm 1$. In the Brillouin zone of the FCC lattice these correspond to the $\Gamma = (0, 0, 0)$, and $X, Y, Z [=2\pi(1, 0, 0)$ and permutations] and four L points [$\pi(1, 1, 1)$ and equivalent points]. These parities are very useful to study the evolution of the band structure. The TRIM parities of the top four occupied bands, in order of increasing energy, are shown in Table 2. Note, although by symmetry all L points are equivalent, the choice of inversion center at an Iridium site singles out one of them, L' . With that choice the parities at the two sets of L points are the opposite of one another. The parities of the all-in/out state remains unchanged above $U > U_c \sim 1.8$ eV, and is shown in the top row under $U = 2$ eV. It is readily seen that these parities arise also for a site localized picture of this phase, where each site has an electron with a fixed moment along the ordering direction. Due to the possibility of such a local description of this magnetic insulator, we term it the Mott phase.

Intermediate Correlations: For the same all-in/out magnetic configuration, at smaller $U = 1.5$ eV, the band structure along high symmetry lines also appears insulating 3b, and at first sight one may conclude that this is an

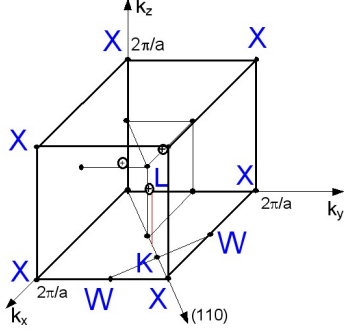


FIG. 5: Brillouin zone of the FCC lattice with locations of Dirac points (shown by + signs denoting their "positive" chiral charges) as found by our LSDA+U+SO calculation with $U=1.5$ eV for $\text{Y}_2\text{Ir}_2\text{O}_7$.

extension of the Mott insulator. However, a closer look at the parities reveals that a phase transition has occurred. A pair of levels with opposite parity are exchanged at the L points. Near this crossing point it can readily be argued that only one of the two adjacent phases can be insulating[30]. Since the large U phase is found to be smoothly connected to a gapped Mott phase, it is reasonable to assume the smaller U phase is the non-insulating one. This is also borne out by the LSDA+U+SO band structure. A detailed analysis perturbing about this transition point (the $k.p$ expansion see [30]) allows us to show that a Dirac semi-metal is expected for intermediate U , with 6 Dirac nodes about every L point. Indeed, in the LSDA+U+SO band structure, we find a 3 dimensional Dirac crossing located within the ΓXL plane of the Brillouin zone. This is illustrated in Fig.5 and corresponds to the k -vector $(0.52, 0.52, 0.3)2\pi/a$. There also are two additional Dirac points in the proximity of the point L related by symmetry. When U increases, these points move toward each other and annihilate all together at the L point close to $U = 1.8$ eV. This is how the Mott phase is born from the Dirac phase. Since we expect that for Ir 5d states the actual value of the Coulomb repulsion should be somewhere within the range $1\text{eV} < U < 2\text{eV}$ we thus conclude that the ground state of the $\text{Y}_2\text{Ir}_2\text{O}_7$ is most likely the semi-metallic state with the Fermi surface characterized by a set of Dirac points but in proximity to a Mott insulating state. Both phases can be switched to a normal metal if Ir moments are collinearly ordered by a magnetic field.

Topological Dirac semi-metal

The effective Hamiltonian in the vicinity of a Dirac momentum $\mathbf{k} = \mathbf{k}_0 + \mathbf{q}$ is:

$$H_D = \sum_{i=1}^3 \mathbf{v}_i \cdot \mathbf{q} \sigma_i \quad (1)$$

, where energy is measured from the chemical potential, and σ_i are the three Pauli matrices. The three velocity vectors \mathbf{v}_i are generically non-vanishing and linearly independent. The energy dispersion is $\Delta E = \pm \sqrt{\sum_{i=1}^3 (\mathbf{v}_i \cdot \mathbf{q})^2}$. Note, by inversion symmetry, there must exist Dirac points at both \mathbf{k}_0 and $-\mathbf{k}_0$, whose velocity vectors are reversed. One can assign a *chirality* (or chiral charge) $c = \pm 1$ to the fermions defined as $c = \text{sign}(\mathbf{v}_1 \cdot \mathbf{v}_2 \times \mathbf{v}_3)$, so Dirac points related by inversion have opposite chirality. Note, since the 2×2 Pauli matrices appear, our Dirac particles are two component fermions. In contrast to regular four component Dirac fermions, it is not possible to introduce a mass gap. The only way to eliminate them is if they meet with another 2 component Dirac dispersion in the Brillouin Zone, but with opposite chiral charge. Thus they are topological objects. We note that near each L point there are three Dirac points related by the three fold rotation, which have the same chiral charge. Fig.5 denotes those points as "+" dots. Another three Dirac points with opposite chirality, related by inversion. Thus, there are 24 Dirac points in the whole Brillouin zone. Since they are all related by symmetry, they are at the same energy. The chemical potential is fixed to be at the Dirac point energy as verified in the microscopic calculation. The Fermi velocities at the Dirac point are found to be typically an order of magnitude smaller than in graphene. We briefly note that this Dirac semimetal is a critical state with power law forms for various properties, which will be described in more detail elsewhere. For example, the density of states $N(E) \propto E^2$. The small density of states makes it an electrical insulator at zero temperature. For a single node with isotropic velocity v , the a.c. conductivity in the free particle limit of the clean system is $\sigma(\Omega) = \frac{e^2}{12h} \frac{|\Omega|}{v} \tanh |\Omega|/4k_B T$.

Surface States: We now discuss surface states that are associated with the presence of the two component Dirac fermions. We first note that they behave like 'magnetic' monopoles of the Berry flux whose charge is given by the chirality. The Berry connection, a vector potential in momentum space, is defined by $\mathcal{A}(\mathbf{k}) = \sum_{n=1}^N i \langle u_{n\mathbf{k}} | \nabla_{\mathbf{k}} | u_{n\mathbf{k}} \rangle$ where N is the number of occupied bands. As usual, an analog of the magnetic field, the Berry flux, is defined as $\mathcal{F} = \nabla_{\mathbf{k}} \times \mathcal{A}$. Now consider energy eigenstates at the Fermi energy (taken to be at $E = 0$). In the bulk, this corresponds to the set of Dirac points, hence the bulk Fermi surface is a collection of

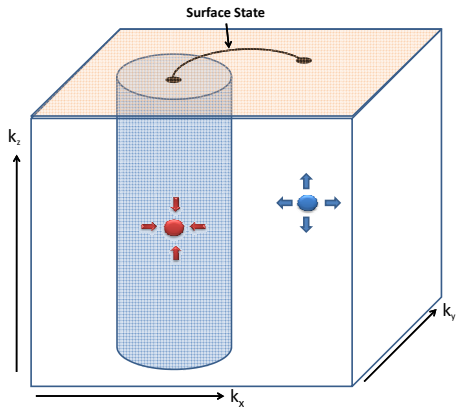


FIG. 6: Illustration of surface states arising from bulk Dirac points. For simplicity, only a pair of Dirac points with opposite chirality are shown. The imaginary cylinder in momentum space has unit Chern number, due to the Berry monopole at the Dirac point. Hence a surface state must arise, as shown schematically in the same plot. When the Fermi energy is at the Dirac point, a Fermi arc is present which connects the surface momenta of the projected bulk Dirac points of opposite chirality.

Fermi points. However, in the presence of a surface (say the plane $z = 0$), new low energy states may be generated. We show that these will occur along a curve in the surface Brillouin zone as is illustrated in Fig. 5. The end points of this curve occur at the bulk Fermi point momenta, projected onto the surface Brillouin Zone. Also, the curve connects Dirac nodes with opposite monopole charge. If more than one Dirac node projects to the same surface momentum, the sum of the monopole charges should be considered. This is argued by showing that there must be Fermi arcs on the surface Brillouin zone emanating from the projection (k_{0x}, k_{0y}) of the monopole as argued below.

Origin of Surface States: We now prove that the band topology associated with the Dirac point leads to surface states. Construct a curve in the surface Brillouin zone encircling the projection of the bulk Dirac point, which is traversed counterclockwise as we vary the parameter $\lambda : 0 \rightarrow 2\pi$; $\mathbf{k}_\lambda = (k_x(\lambda), k_y(\lambda))$ (see Fig. 6). We show that the energy ϵ_λ of a surface state at momentum \mathbf{k}_λ crosses $E = 0$. Consider $H(\lambda, k_z) = H(\mathbf{k}_\lambda, k_z)$, the gapped Hamiltonian of the two dimensional subsystem defined by this curve. The two periodic parameters λ, k_z define the surface of a torus in momentum space (see Fig. 6). The Chern number of this two dimensional band structure is given by the Berry curvature integration: $\frac{1}{2\pi} \int \mathcal{F} dk_z d\lambda$ which, by Stokes theorem, simply corresponds to the net monopole density enclosed within the torus. This is obtained by summing the chiralities of the enclosed Dirac nodes. Consider the case when the

net chirality is unity, corresponding to a single enclosed Dirac node. Then, the two dimensional subsystem defines a quantum Hall insulator with unit Chern number. When defined on the half space $z < 0$, this corresponds to putting the quantum Hall state on a cylinder, and hence we expect a chiral edge state. Its energy ϵ_λ spans the band gap of the subsystem, as λ is varied. Hence, this surface state crosses zero energy somewhere on the surface Brillouin zone \mathbf{k}_{λ_0} . Such a state can be obtained for every curve enclosing the Dirac point. Thus, at zero energy, there is a Fermi line in the surface Brillouin zone, that terminates at the Dirac point momenta (see Fig. 6). An arc beginning on a Dirac point of chirality c has to terminate on a Dirac point of the opposite chirality. Clearly, the net chirality of the Dirac points within the (λ, k_z) torus was a key input in determining the number of these states. If Dirac points of opposite chirality line up along the k_z direction, then there is a cancelation and no surface states are expected.

For $U = 1.5$ eV, a Dirac node is found to occur at the momentum $(0.52, 0.52, 0.31)2\pi/a$ and equivalent points (see Fig.3). They can be thought of as occurring on the edges of a cube, with a pair of Dirac nodes of opposite chirality occupying each edge, as, e.g., the points $(0.52, 0.52, 0.31)2\pi/a$ and $(0.52, 0.52, -0.31)2\pi/a$. For the case of $U = 1.5$ eV, the sides of this cube have the length $0.52(4\pi/a)$. Thus, the (111) and (110) surfaces would have surface states connecting the projected Dirac points. If, on the other hand we consider the surface orthogonal to the (001) direction, it would lead to the Dirac points of opposite chirality being projected to the same surface momentum, along the edges of the cube. Thus, no protected states are expected for this surface.

Model Calculation: To verify these theoretical considerations, we have constructed a tight binding model which has features seen in our electronic structure calculations for YIr_2O_7 . We consider only t_{2g} orbitals of Ir atoms in the global coordinate system. Since Ir atoms form tetrahedral network (see Fig. 2), each pair of nearest neighboring atoms forms a corresponding σ -like bond whose hopping integral is denoted as t and other two π -like bonds whose hopping integrals are denoted as t' . To simulate the appearance of the Dirac point it is essential to include next-nearest neighbor interactions between t_{2g} orbitals which are denoted as t'' . With the parameters $t = 0.2, t' = 0.5t, t'' = -0.2t$, the value of the on-site spin-orbit coupling equal to $2.5t$ and the applied on-site splitting between spin up and spin down states equal to 0.1 referred to the local quantization axis which simulates our non-collinear 'all-in/out' configuration we can model both the bulk Dirac metal state and its surface. The calculated (110) surface band structure for the slab of 128 atoms together with the sketch of the obtained Fermi arcs is shown in Fig. 7. Notice that since the slab calculation involves two surfaces, the corresponding surface states and Fermi arcs for both surfaces are generated.

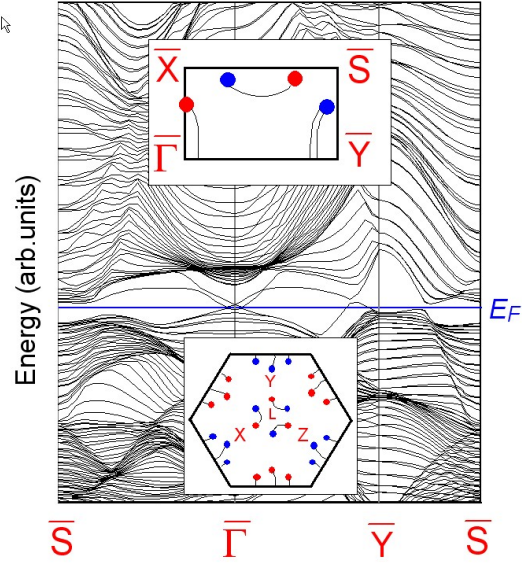


FIG. 7: Calculated surface energy bands corresponding to (110) surface of the pyrochlore iridate $\text{Y}_2\text{Ir}_2\text{O}_7$. A tight binding approximation has been used to simulate the bulk band structure with 3D Dirac point as found by our LSDA+U+SO calculation. The plot corresponds to diagonalizing 128 atoms slab with two surfaces. The top inset shows the deduced Fermi arcs connecting projected bulk Dirac points of opposite chirality. The bottom inset shows a sketch how these Fermi arcs are expected to behave for the (111) surface.

We also display the expected surface states for the (111) surface. Note, no special surface states are expected for the (001) surface.

OTHER TOPOLOGICAL PHASES

We recall that topological insulators are non-magnetic band insulators with protected surface states [6]. Time reversal symmetry is required in the bulk to define these phases. When the surface states are eliminated by adding, for example magnetic moments only on the surface, a quantized magneto-electric response is obtained, where a magnetic field induces a polarization: $\mathbf{P} = \theta \frac{e^2}{2\pi h} \mathbf{B}$, with the coefficient $|\theta|$ [15] is only defined modulo 2π . Under time reversal, $\theta \rightarrow -\theta$. Apart from the trivial solution $\theta = 0$, the ambiguity in the definition of θ allows also for $\theta = \pi$. For topological insulators $\theta = \pi$.

In magnetic insulators, θ is in general no longer quantized [26]. However, when inversion symmetry is retained, θ is quantized again, since inversion also changes its sign. Thus again $\theta = 0, \pi \bmod 2\pi$, and an insulator with the latter value will be termed a $\theta = \pi$ axion insulator.

Which is the appropriate description of the pyrochlore

iridate phases we have described? For the Mott insulator, at large U , the charge physics must be trivial and so we must have $\theta = 0$. Next, since the Dirac semi metal phase is gapless in the bulk, θ is ill defined. However, we note that on reducing U , the location of the Dirac points shift, with nodes of opposite chirality approaching each other. If these meet and annihilate, then one recovers a gapped phase in the low U regime. However, in the process the resulting phase will have $\theta = \pi$. Indeed, the presence of the intervening Dirac phase can be deduced from the requirement that θ has to change between these two quantized values. As described elsewhere[25], the condition for $\theta = \pi$ when deduced from the parities, turns out to be the same as the Fu-Kane formula, for time reversal symmetric insulators [27, 28], i.e. if the total number of filled states of negative parity at all TRIMs taken together is twice an odd integer, then $\theta = \pi$. Otherwise $\theta = 0$. The small U insulator has the same parities as the Dirac semi-metal, since the Dirac points annihilate away from a TRIM. From Table II we can see that indeed this corresponds to $\theta = \pi$, since there are 14 negative parity filled states, while the Mott insulator corresponds to $\theta = 0$, having 12 negative parity filled states.

Unfortunately, within our LSDA+U+SO calculation, a metallic phase intervenes on lowering $U \leq 1.0\text{eV}$, before the Dirac points annihilate to give the axion insulator. We point out this possibility nevertheless, since LDA systematically underestimates the stability of such gapped phases. Moreover it provides an interesting example of a pair of insulators with the same magnetic order, but which are nevertheless different phases. Thus, the Mott insulator is distinct from the smaller U ‘Slater’ insulator, unlike in many other cases where they are smoothly connected to one another. Inversion symmetry is critical in preserving this distinction.

In summary, a theoretical phase diagram for the physical system is shown in Figure 1 as a function of U and applied magnetic field, which leads to a metallic state beyond a critical field. The precise nature of these phase transformations are not addressed in the present study

ACKNOWLEDGEMENTS

A.V. thanks L. Balents, J. Orenstein and R. Ramesh for insightful discussions. X.W. acknowledges support by National Key Project for Basic Research of China (Grant No. 2006CB921802, and 2010CB923404), NSFC under Grant No. 10774067, and 10974082. S.S. acknowledges support by DOE SciDAC Grant No. SE-FC02-06ER25793 and thanks Nanjing University for the kind hospitality during his visit to China. X.W. and S.S. also acknowledge support from Kavli Institute for Theoretical Physics where this work has been initiated. The work at Berkeley was supported by the Office of Basic Energy Sciences, Materials Sciences Division of the U.S. Depart-

ment of Energy under contract No. DE-AC02-05CH1123.

APPENDIX

I. Effective $\mathbf{k}\cdot\mathbf{p}$ Theory and Intervening Dirac Metal Phase

Consider a pair of states at the L point which have opposite parity, and cross each other as we tune U . We want to understand what happens to the band structure.

The L point has two symmetries which do not change its crystal momentum. First of course is inversion, and we can label states by the eigenvalues $P = \pm 1$. The second is 120° rotations about a line joining $L-\Gamma$. There are three possible eigenvalues which we call $s = -1/2, 1/2, 3/2$. So, any state at this point can be labeled by $\{P, s\}$. Now consider writing the effective 2×2 Hamiltonian for a pair of states that are near each other in energy:

1. *At the L point:* Since we have inversion symmetry, the two states taken to be eigenvalues of $\tau_z = \pm 1$, cannot mix. Hence the effective Hamiltonian is

$$H(L) = \Delta \tau_z$$

where the coefficient Δ changes sign when the levels pass through each other. Note, the s quantum number of the two levels is irrelevant here.

2. *Along the $\Gamma - L$ Direction:* We still have the quantum number s , but not P , since that inverts the momentum. Denoting by k_z the momentum along this line deviating from the L point, we have two cases. If the s quantum number of the two levels is different, they still cannot mix, so the effective Hamiltonian is $H = (\Delta + k_z^2)\tau_z$. Now, when $\Delta < 0$ there are two solutions $k_z = \pm\sqrt{-\Delta}$, where there are nodes along this $\Gamma - L$ line. You can see this for the $s = 1/2$ and $s = 3/2$ crossings in the data.

However, if the states have the *same* s quantum number they can mix, once you move away from L . Now the effective Hamiltonian is:

$$H(\Gamma - L) = (\Delta + k_z^2)\tau_z + k_z\tau_x$$

where the second term arises since inversion is broken on moving away from L allowing for mixing. Now, the spectrum is $E = \sqrt{(k_z^2 - |\Delta|)^2 + k_z^2}$, for $\Delta < 0$, so despite a level crossing there is no node along the $\Gamma - L$ line.

3. *General Point in BZ:* In the latter case, does this mean there are no Dirac points? No - we just need to move off the $\Gamma - L$ line. Let the deviation be \mathbf{k}_\perp , a 2 vector. The fact the 2 levels have opposite parity means we need an odd function of k_\perp to

induce a matrix element between the levels. And also, since \mathbf{k}_\perp is a 2 vector, it transforms under the rotation - the rotationally symmetric form allowed is $\Delta H = k_\perp^3 \cos 3\theta \tau_x + k_\perp^3 \sin 3\theta \tau_y$. Putting this all together we have the effective Dirac Hamiltonian near the L point:

$$H(\mathbf{k}) = (\Delta + k_z^2)\tau_z + (k_z + k_\perp^3 \cos 3\theta)\tau_x + k_\perp^3 \sin 3\theta \tau_y$$

Note, this has the form $A(k)\tau_z + B(k)\tau_x + C(k)\tau_y$. For a node, $A = B = C = 0$. This occurs if: $A = 0$ so $k_z = +\sqrt{-|\Delta|}$, and $C = 0$ implies $\theta = p\pi/3$, where p is an integer; and finally $k_\perp^3 = k_z$, when $p = 1, 3, 5$. Similarly for $k_z < 0$, the nodes are inverted. In all we have 6 nodes for this L point, 24 Nodes in all.

Actually this is not the complete expansion. Strictly we should write $A(k) = m + k_z^2 + \alpha k_\perp^2$. This is an effective mass Hamiltonian near the L point. If $\alpha > 0$, then it turns out the conclusions are the same as above, without this additional term (i.e., there is a transition from $\theta = \pi$ magnetic axion insulator to Dirac metal on increasing U). *However*, if $\alpha < 0$, this completely changes the conclusions, as discussed below. In fact, this turns out to be the physically relevant case according to the electronic structure calculations for $\text{Y}_2\text{Ir}_2\text{O}_7$.

Let us assume $\alpha = -1/m_2 < 0$. Then the effective Hamiltonian:

$$H(\mathbf{k}) = (\Delta + \frac{k_z^2}{2m_1} - \frac{k_\perp^2}{2m_2})\tau_z + (\beta k_z + k_\perp^3 \cos 3\theta)\tau_x + k_\perp^3 \sin 3\theta \tau_y \quad (2)$$

where a few parameters have been labeled. The Dirac nodes then are at: (i) $C = 0 \rightarrow \theta = p\pi/3$ and (ii) using this, $B = 0 \rightarrow k_z = \pm k_\perp^3/\beta$ depending on whether we look at $p = \text{odd}$ or $p = \text{even}$. Finally, using these relations we have for $A = 0$ equation:

$$\Delta + \frac{k_\perp^6}{2\beta^3 m_1} - \frac{k_\perp^2}{2m_2} = 0$$

for small Δ this has the solution $k_\perp^2 = 2m_2\Delta$. Note, this has a solution only for $\Delta > 0$, i.e. before the gap gets inverted at the L point on increasing U . Thus, in this scenario, there is a Dirac point only in the small U phase. These Dirac points live along $\theta = p\pi/3$ plane, which is the $k_x = k_y$ plane that contains the points $\Gamma - L - K$ and rotations thereof.

II. Summary of Experiments

We now summarize the experimental facts about the pyrochlore iridates $\text{A}_2\text{Ir}_2\text{O}_7$. Early work revealed that increasing the A ion radius triggered a metal-insulator

transition in the ground state. Thus while $A = \text{Pr}$ is metallic, $A = \text{Y}$ is insulating at low temperatures [11]. Reducing the ionic radius is believed to narrow the bandwidth and increase correlations. Subsequent improvement in sample quality revealed that $A = \text{Eu}$, Sm , Nd also displayed low temperature insulating states [13]. In these systems, a metal insulator transition is clearly observed on cooling (eg. at $T_{MI} = 120\text{K}$ for $A = \text{Eu}$). At the same temperature, a signature in magnetic susceptibility is also observed, indicative of a magnetic transition [12]. This magnetic signature, wherein the field cooled and zero field cooled magnetic susceptibilities separate below the transition temperature, is reminiscent of a spin glass state. Since this signature is seen in $A = \text{Y}$, Lu [12], with nonmagnetic A site atoms, it is associated with Ir site moments. In $\text{Y}_2\text{Ir}_2\text{O}_7$, no sharp resistivity signature has been reported at the magnetic transition, but the resistivity climbs steeply on cooling below this temperature. Moreover, light hole doping suppresses both the insulating state and the magnetic transition [23]. Finally, we note that a thermodynamic signature of the magnetic transition, a bump in the specific heat, is observed in clean samples of $A = \text{Sm}$ [13]. X-ray scattering did not observe any structural change below the ordering transition [13], although the presence of new lines in the Raman spectroscopy [29] has been attributed to lowering of cubic symmetry in $A = \text{Eu}$, Sm but not in $A = \text{Nd}$.

We now discuss how the present theoretical description sits with these facts. We propose that the low temperature state of $\text{Y}_2\text{Ir}_2\text{O}_7$ (and also possibly of $A = \text{Eu}$, Sm and Nd iridates) is the Dirac semi-metal, with all-in/all-out magnetic order. This is broadly consistent with the interconnection between insulating behavior and magnetism observed experimentally. It is also consistent with being proximate to a metallic phase on lowering the correlation strength, such as $A = \text{Pr}$. In the clean limit, a three dimensional Dirac semi-metal is an electrical insulator, and can potentially account for the observed electrical resistivity. The noncollinear magnetic order proposed has Ising symmetry and could undergo a continuous ordering transition. Since this configuration is not frustrated, it is not clear how spin glass behavior would arise, but the observed magnetic signature could perhaps also arise from defects like magnetic domain walls. A direct probe of magnetism is currently lacking and would shed light on this key question.

[1] J. Orenstein and A. J. Millis, Science 288, 468 - 474 (2000)
 [2] Y. Tokura and N. Nagaosa, Science 288, 462-467 (2000)

[3] B.J. Kim, *et al.*, Phys. Rev. Lett. **101**, 076402 (2008), B.J. Kim, H. Ohsumi, T. Komesu, S. Sakai, T. Morita, H. Takagi, and T. Arima, Science **323**, 1329 (2009).
 [4] Y. Okamoto, M. Nohara, H. Aruga-Katori, and H. Takagi, Phys. Rev. Lett. **99**, 137207 (2007).
 [5] P.A. Lee, Science **321**, 1306 (2008); L. Balents, Nature (London) **464**, 199 (2010).
 [6] M.Z. Hasan and C.L. Kane, arXiv:1002.3895 (2010). J. E. Moore, Nature 464(7286):194-8 (2010). X. Qi and S. C. Zhang, Physics Today 63, 33 (2010).
 [7] A. Shitade, H. Katsura, J. Kuneš, X.-L. Qi, S.-C. Zhang, and N. Nagaosa, Phys. Rev. Lett. **102**, 256403 (2009).
 [8] D. A. Pesin, L. Balents, Nature Physics 6, 376 - 381 (2010).
 [9] M.A. Subramanian, G. Aravamudan and G.V. Subba Rao, Prog. Solid St. Chem. **15**, 55 (1983); S.T. Bramwell and M.J.P. Gingras, Science **294**, 1495 (2001); A.P. Ramirez, Ann. Rev. Mater. Sci. **24**, 453 (1994).
 [10] J. S. Gardner, M. J. P. Gingras, J. E. Greedan, Rev. Mod. Phys. **82**, 53 (2010).
 [11] D. Yanagishima, and Y. Maeno, J. Phys. Soc. Jpn. **70**, 2880 (2001).
 [12] N. Taira, M. Wakeshima and Y. Hinatsu, J. Phys.: Condens. Matter **13**, 5527 (2001).
 [13] K. Matsuhira, M. Wakeshima, R. Nakanishi, T. Yamada, A. Nakamura, W. Kawano, S. Takagi, and Y. Hinatsu, J. Phys. Soc. Jpn. **76**, 043706 (2007).
 [14] A. K. Geim and K. S. Novoselov, Nature Materials 6, 183 - 191 (2007).
 [15] X. Qi, Taylor Hughes and S. C. Zhang, Phys. Rev. B 78, 195424 (2008).
 [16] Frank Wilczek, Phys. Rev. Lett., **58**, 1799 (1987).
 [17] K. Maiti, Solid State Commun. **149**, 1351 (2009).
 [18] B. J. Yang and Y. B. Kim, arxiv/1004.463.
 [19] S. Y. Savrasov, Phys. Rev. B **54**, 16470 (1996).
 [20] V.I. Anisimov, F. Aryasetiawan, and A.I. Lichtenstein, J. Phys.: Condens. Matter **9**, 767 (1997).
 [21] R. Siddharthan, B.S. Shastry, A.P. Ramirez, A. Hayashi, R.J. Cava, and S. Rosenkranz, Phys. Rev. Lett. **83**, 1854 (1999); M.J. Harris, S.T. Bramwell, D.F. McMorrow, T. Zeiske, and K.W. Godfrey, Phys. Rev. Lett. **79**, 2554 (1997).
 [22] M. Elhajal, B. Canals, R. Sunyer and C. Lacroix, Phys. Rev. B **71**, 094420 (2005).
 [23] H. Fukazawa and Y. Maeno, J. Phys. Soc. Jpn. **71**, 2578 (2002); M. Soda, N. Aito, Y. Kurahashi, Y. Kobayashi, M. Sato, Physica B **329**, 1071 (2003).
 [24] H.-M. Guo and M. Franz, Phys. Rev. Lett **103**, 206805 (2009).
 [25] Ari M. Turner, Yi Zhang and Ashvin Vishwanath, to appear.
 [26] Essin, A. M., Moore, J. E. and Vanderbilt, D., Phys. Rev. Lett. 102, 146805 (2009).
 [27] Liang Fu and C. L. Kane, Phys. Rev. B 76, 045302 (2007).
 [28] Z. Wang, X.L. Qi, S. C. Zhang, New J. Phys. 12, 065007 (2010).
 [29] T. Hasegawa *et al.*, Journal of Physics: Conference Series 200 012054, (2010).
 [30] See Appendix.